Rotamers of Isoprene: Infrared Spectroscopy in Helium Droplets and Ab Initio Thermochemistry

Peter R. Franke and Gary E. Douberly*

Department of Chemistry, University of Georgia, Athens, Georgia 30602-2556

*Corresponding Author

Email: douberly@uga.edu; Tele: 01-706-542-3857

Abstract

Isoprene (C₅H₈) is an abundant, reactive tropospheric hydrocarbon, derived from biogenic emissions. A detailed understanding of the spectroscopy of isoprene is therefore desirable. Isoprene monomer is isolated in helium droplets and its infrared spectrum is measured in the CH stretching region. Anharmonic frequencies are predicted by VPT2+K simulations employing CCSD(T) force fields with quadratic (cubic and quartic) force constants computed using the ANO1 (ANO0) basis set. The vast majority of the spectral features can be assigned to *trans*-isoprene on the basis of these computations. Some features of the higher energy *gauche* conformer are also assignable, by comparison to experiments using heated isoprene. Convergent *ab initio* thermochemistry is presented for the isomerization pathway, for which the partition function explicitly accounts for the eigenstates associated with separate, uncoupled one-dimensional potential surfaces for methyl torsion and internal rotation between rotamers. The respective 0 K and 298.15 K *trans/gauche* energy differences are 2.82 and 2.52 kcal/mol, which implies a room temperature *gauche* population of 2.8%.

1

1. Introduction

Isoprene annually comprises ~500 Tg of biogenic emissions into the troposphere, which represents 44% of total emissions of non-methane volatile organic compounds (VOCs).¹ Isoprene has a daytime half-life of less than 2 hours, and its oxidation is the dominant source of summertime tropospheric ozone.²⁻³ Indeed, accurate models of tropospheric oxidative capacity will demand a thorough understanding of the OH initiated oxidation of isoprene and monoterpenes, which is still incomplete.^{1,4} Moreover, isoprene is believed to be a significant contributor to secondary organic aerosol (SOA) formation via pathways beginning with the OH addition reaction.⁵⁻¹⁰ Isoprene-derived SOA influences the global radiation budget and can act as cloud condensation nuclei. 11 The tropospheric chemistry of isoprene is initiated largely by the electrophilic addition of OH to double bonds, leading to hydroxyalkyl adduct formation. These adducts react with O₂, forming hydroxyperoxy radicals, which are involved in a series of complex reaction pathways leading to a variety of products. 12-13 Because isoprene is the starting point for these complex oxidation pathways, an accurate determination of its conformer populations (trans and gauche) is necessary, as different conformers may follow different pathways. 13 In this report, we present a detailed analysis of the infrared (IR) spectrum in the CH stretching region and analyze the spectral complexity that emerges due to the anharmonic coupling of stretching fundamentals and bending overtone/combination states. Moreover, convergent theoretical thermochemistry for the isomerization pathway is presented.

The IR spectrum of isoprene has been measured in the gas phase at room temperature¹⁴ and in Ar¹⁴ and N₂ matrices.¹⁵ However, a spectrum that is simultaneously cold and minimally-perturbed, with sub-wavenumber resolution, is currently absent from the literature.

Measurements of cold, vibrationally-resolved spectra are expected to reveal the multitude of

bending overtone and combination bands that cohabitate with CH stretch fundamentals, particularly in the region from 2800 to 3000 cm⁻¹. ¹⁶ This region is home to groups of strongly-interacting vibrational states, called polyads, of which the complexity grows rapidly with the size of the molecule. ¹⁷⁻¹⁹ This provides challenging test cases for anharmonic theory. ²⁰ The helium nanodroplet isolation technique allows for the acquisition of the vibrationally-resolved IR spectrum of isoprene in the CH stretching region. Indeed, the low temperature and weak matrix interactions afforded by this technique yield a spectrum whose analysis requires an explicit treatment of anharmonic coupling. ¹⁶ Here we apply the VPT2+K approach in a normal mode representation, ²¹ which provides a detailed picture of the polyad structure associated with this wavelength region.

To our knowledge, the highest level theoretical study of isoprene's rotamers was reported by Allodi *et. al.*¹³ Their investigation was focused on the various OH-addition adducts and pre-reactive complexes, but they also studied the *trans/gauche* isomerization potential of isoprene at the CCSD(T)/aug-cc-pVTZ//BHandHLYP/6-311G** level of theory. The lowest lying conformer was the familiar *trans* structure, and the enthalpy for interconversion to the *gauche* structure, ΔH_0 , was predicted to be 2.66 kcal/mol.¹³ On the basis of a theoretical ΔG_{298} of 2.45 kcal/mol, the *trans* structure was determined to be far more abundant (96.8%) at 298.15 K than the higher energy *gauche* structure (3.2%). Squillacote and Liang¹⁵ computed thermochemical parameters with the G3 composite method for various methyl-substituted dienes, including isoprene ($\Delta H_0 = 2.73$ kcal/mol). These authors also derived an experimental interconversion enthalpy (2.46 kcal/mol) from a van't Hoff analysis of solid-N₂ matrix isolation spectra. Here we apply convergent electronic structure theory (*i.e.* focal point analysis)²²⁻²⁴ to improve upon

the previously reported theoretical thermochemistry, which includes explicit analysis of the partition functions associated with methyl torsion and the *trans/gauche* interconversion pathway.

2. Experimental Methods

Details of the helium droplet methodology can be found elsewhere. ²⁵⁻²⁶ Ultrapure (99.9995%) helium at 35 bar is continuously expanded through a 5 μm, 17 K nozzle to form He nanodroplets, producing a distribution of droplets containing 4000-6000 He atoms on average. ²⁷ Droplets are skimmed into a beam and passed into a second vacuum chamber and through a pick up cell (PUC). Vapor from a glass bulb of liquid isoprene (99%, Sigma Aldrich) is metered into the PUC. Helium droplets collide with gas phase isoprene molecules; and following solvation, the molecules are rapidly cooled to the droplet temperature of ~0.4 K. ²⁵⁻²⁶ The PUC pressure is adjusted to be less than that necessary to optimize single molecule pick up. Based on the Poisson capture statistics ²⁸ and the log-normal distribution of droplet sizes, ²⁷ 18% of the droplet ensemble is doped with isoprene monomer, and 2.3% of the droplet ensemble picks up two isoprene molecules that cluster within the droplet to form an isoprene dimer. A negligible fraction of the ensemble picks up three or more isoprene molecules.

After being doped, the droplet beam interacts with the mid-IR beam of an optical parametric oscillator (OPO), which propagates antiparallel to the droplet beam. The tuning and calibration of this laser system are discussed elsewhere.²⁹ Upon excitation, the vibrational energy of the molecule is quenched by the evaporation of He atoms from the droplet.

Evaporation of one helium atom carries away approximately 5 cm⁻¹ of vibrational energy.³⁰ Loss of helium reduces the average geometric cross section of the droplets, decreasing the cross section for electron impact ionization, which is detected with a quadrupole mass spectrometer

tuned to pass only ions within a particular mass channel. The IR beam is mechanically chopped at 80 Hz, and the ion current is processed with a lock-in amplifier. The resulting IR spectrum is a laser on *vs.* laser off difference spectrum associated with the chosen mass channel, and the signal is normalized to the power of the laser beam. The mass spectrometry scheme by which action spectra are recorded and the choice of mass channel is discussed in detail in the Supporting Information (see Figure S1).

For temperature-dependence experiments, the gas phase isoprene was heated within the PUC to increase the population of the higher energy rotamer while maintaining a fixed number density of isoprene molecules within the PUC. This was accomplished by tightly packing the PUC with copper wool, two 125 Watt cartridge heaters, and a K-type thermocouple. Gas-phase isoprene molecules had to pass through the copper wool prior to interacting with the droplet beam. Variable current was applied to the cartridge heaters, and the temperature of the isoprene was taken from the thermocouple reading (~700 K). Previous studies of multi-conformer systems have shown that the gas-phase conformer ratio is preserved upon helium solvation, ³¹⁻³² because the helium cooling is sufficiently rapid such that interconversion is prevented within the droplet. We note that thermal equilibration by collisions with the hot copper wool in the PUC prior to droplet pick up is not essential in our analysis. In general, we find that the CH stretching region is too congested to provide highly accurate trans: gauche intensity ratios. Therefore, our scheme is simply set up to enhance the population of the higher energy gauche rotamer to aid in its spectral assignment, and we do not attempt here to vary the PUC temperature and derive an experimental enthalpy of interconversion via van't Hoff analysis of the trans: gauche conformer ratio.

3. Theoretical Methods

3.1 Relative Enthalpy

Four stationary points were characterized: a C_s electronic minimum (trans) and first-order saddle point (cis), and a C_I electronic minimum (gauche) and first-order saddle point. Geometries were optimized using the CCSD(T)³³⁻³⁸ method combined with the ANO0 and ANO1 basis sets, ³⁹ as implemented in CFOUR. ⁴⁰ Unless otherwise noted, the frozen-core approximation was made, i.e. the carbon 1s electrons were not included in the post-HF treatment. Energies were obtained at the CCSD(T)/ANO1 geometries by extrapolation to the complete basis set limit. The HF-SCF energy was extrapolated with a 3-point formula from cc-pVXZ (X = 4,5,6) energy calculations. ⁴¹ The correlation energies were extrapolated using a 2-point formula from cc-pVXZ (X = 4,5,6) energy calculations energy calculations. ⁴² The points used in the correlation energy extrapolations were those with the largest basis sets: X = 5,6 for MP2, X = 4,5 for CCSD, and X = 3,4 for CCSD(T). All energy calculations used in extrapolations were performed in Gaussian 09, ⁴³ while energy calculations using the ANO0 basis were performed in CFOUR.

The anharmonic ZPVE, excluding contributions from the isomerization and methyl torsion modes, was computed using a resonance-free formula. 44 The zero-point energies associated with the methyl torsion and isomerization coordinates were determined by 1D variational solutions of relaxed CCSD(T)/ANO1//CCSD(T)/ANO0 potentials using the procedure of Laane and coworkers. 45-46 The methyl torsion is allowed to relax in the isomerization potential; however, the skeletal torsion is frozen in the methyl torsional potentials. It follows from this that the coupling between the two coordinates is largely ignored. Three additional corrections were appended to the CCSD(T)/CBS energies. First, the effects of core correlation were accounted for by differencing all-electron and frozen-core energies using

CCSD(T) with the cc-pCVTZ basis set.⁴⁷ Secondly, diagonal Born-Oppenheimer corrections (DBOC) were computed at the HF/ANO1 level of theory.⁴⁸⁻⁴⁹ Finally, corrections for post-CCSD(T) electron correlation effects were added. CCSDT(Q) energies were computed only with the ANO0 basis set, and the [CCSDT/ANO0 - CCSD(T)/ANO0] and [CCSDT(Q)/ANO0 – CCSDT/ANO0] increments were assumed to be additive. These are included in the focal point tables (Tables 1, 2, and 3) alongside the extrapolated energies.

Previous work has shown that the higher-order electron correlation correction can be expected to be reasonably close to the basis set limit, even with small basis sets such as ANO0.⁵⁰⁻⁵² CCSDT(Q)⁵³⁻⁵⁵ energy calculations were performed using the MRCC program.⁵⁶ This scheme for evaluating the electronic energies is a form of focal point analysis (FPA) originally proposed by Allen and coworkers.²²⁻²⁴

3.2 Relative Free Energy

The aforementioned focal point analysis and anharmonic ZPVE treatment provides the *trans/gauche* interconversion enthalpy at zero Kelvin. To compute the free-energy at 298.15 K, a fairly traditional analysis was conducted.⁵⁷ Due to the nature of the structures being compared, relative free-energy requires only that the rotational entropy, vibrational entropy, and vibrational thermal energy contributions be evaluated. Free energy of isomerization is defined as:

$$\Delta G = \Delta H + \Delta E_{vib} - T(\Delta S_{vib} + \Delta S_{rot}),$$

where ΔH represents the 0 K enthalpy and ΔE_{vib} is relative to v=0, *i.e.* it does not include the zero-point energy. The rigid-rotor approximation was invoked for the rotational entropy. The harmonic oscillator approximation was used for the vibrational thermal energy and entropy of the 3N-8 highest vibrational degrees of freedom. We decided against an anharmonic treatment of

the ΔE_{vib} and ΔS_{vib} terms due to challenges associated with accounting for resonances and the observation that nearly half of all 298.15 K thermal contributions are derived from the torsional modes. For the isomerization and methyl torsion degrees of freedom, partition functions were computed by a direct eigenstate count from the torsional potentials (see Figures S2, S3, S4, S5, and S6). In the instance of methyl torsion, a factor of 1/3 appears in front of the partition function expressions, given by:

$$Q_{tors}^{CH_3}(T) = \frac{1}{3} \sum_{n=1}^{\infty} e^{\left(-\frac{E_n - E_1}{k_B T}\right)}$$

This is because the torsional motion interconverts three indistinguishable versions of isoprene. Eigenstates were summed until the partition functions converged.

Calculating the skeletal torsional partition function for the *trans* conformer is straightforward. All eigenstates localized in the *trans* well were counted. In the energy regime above the *trans-gauche* barrier, where the eigenstates are nearly degenerate pairs, all states were counted toward both *trans* and *gauche*. At 298.15 K, the contribution of these levels to the *trans* partition function is minimal. The distinguishable (enantiomeric) nature of the *gauche* conformers can be accounted for in two equivalent ways. First, the enantiomers can be considered separately. All *gauche* eigenstates can be summed, and a factor of 1/2 can be introduced in front of the *gauche* skeletal torsional partition function to prevent overcounting. The fraction of *gauche* isoprene is calculated as:

$$\frac{2e^{\left(-\frac{\Delta G}{k_{\rm B}T}\right)}}{1+2e^{\left(-\frac{\Delta G}{k_{\rm B}T}\right)}}$$

This is the approach used in this study. Alternatively, the *gauche* enantiomers can be considered together, from the beginning, leaving out the 1/2 factor. This is intuitively more appealing at high

temperatures, where large fractions of *gauche*-isoprene would be found in excited skeletal torsional states lying above the *gauche-gauche* barrier (cis). With this approach, the calculated ΔG is lower and can be interpreted as a *trans-cis* free-energy difference. The fraction of higher energy conformers is then calculated as:

$$\frac{e^{\left(-\frac{\Delta G}{k_{\rm B}T}\right)}}{1+e^{\left(-\frac{\Delta G}{k_{\rm B}T}\right)}}$$

where the factors of 2 are now absent. Both approaches differ only in their interpretation. They give identical population ratios. Subsequently, all thermodynamic quantities were computed directly from the torsional partition functions using standard expressions.⁵⁷ Much of this information is provided in the Supporting Information (Table S1, S2, S3, and S4).

3.3 Anharmonic Theory

The local mode Hamiltonian model developed by Sibert and coworkers is an appealing approach for dealing with anharmonic coupling in the CH stretch spectral region. ^{16, 18-20} However, their model relies upon parameterization. To our knowledge, Sibert's local mode model in its current form cannot handle the CH stretch / (C=C stretch + HCH bend) interactions that are so important (*vide infra*) for isoprene and indeed for other unsaturated hydrocarbons. ⁵⁸ Predictions of the isoprene vibrational spectra were made using the VPT2+K method. ^{21, 59-61} Quadratic force constants and first derivatives of the dipole moment were computed at CCSD(T)/ANO1 by numerical differentiation of analytic gradients. Cubic and semi-diagonal quartic force constants were computed by numerical differentiation of CCSD(T)/ANO0 analytic second derivatives. ⁶² These force constants were combined into a hybrid force field. ¹⁷ The standard VPT2 procedure was carried out, using scripts written in Mathematica 11. ⁶³

Similar effective Hamiltonians were built for both trans and gauche conformers. All of the CH stretching fundamentals were included (8 states). Then 2-quanta vibrational states were chosen in a systematic way, on the basis of zeroth-order energies and Martin diagnostic values.⁶⁴ The Martin diagnostic used here is not the approximate formula; rather, it is the exact difference between the second-order perturbation theory correction and the variational correction resulting from a 2-state interaction.⁶⁴ All possible 2-quanta states were built from the following 9 normal coordinates: three CH₃ scissors, two CH₂ scissors, one CH in-plane bend, one skeletal bend, and the symmetric and antisymmetric C=C stretches (45 states). The complete list of normal modes is available in Table 4. The diagonal elements of the effective Hamiltonian were the VPT2 frequencies of each state, deperturbed for interactions with all other states within the effective Hamiltonian. Off-diagonal matrix elements involve cubic and quartic force constants and provide explicit Fermi and Darling-Dennison couplings. Diagonalization of the effective Hamiltonian yields the anharmonic transition frequencies. Anharmonic intensities are determined from the CCSD(T)/ANO1 harmonic intensities, where the intensity of each anharmonic transition is simply proportional to the fraction of each zeroth-order CH stretching state that it contains.

Connected resonances are also present in these systems. These can complicate the polyads, and they require more careful treatment. These are instances where a fundamental of one of the 9 normal coordinates that were selected to populate the list of 2-quanta states is in Fermi resonance with some further 2-quanta state. This 2-quanta state is typically characterized by skeletal bending and/or CH wagging/rocking/twisting. This resonance affects the energies of the 2-quanta states in the effective Hamiltonian, which in-turn affects the 1-quantum CH stretches. Correction for this necessitates the addition of 3-quanta states to the effective Hamiltonian. The Martin diagnostic with a threshold of 1 cm⁻¹ was used to identify such

connected resonances: 7 are found for *trans* and 5 are found for *gauche*. By inspection of the normal modes involved in each resonance, 3 of them are found to involve very closely the same motions in both conformers. It was endeavored to make the simulations for both conformers comparable, so as to facilitate a fair comparison of band positions. Based on further comparisons of the normal modes, 2 resonances were added to the *trans* list, and 4 were added to the *gauche* list, bringing the total to 9 connected resonances apiece (72 states).

Identified resonances involving torsionally-excited states were ignored; these interactions were kept perturbed. This practice was helpful for reducing the complexity of the effective Hamiltonian; and in our experience, there really is no good way to handle torsions within the framework of VPT2+K. However, very large Martin diagnostic values for these stretch-torsion couplings should be a cause for concern. The Martin diagnostic does not turn up any strong (> 10 cm⁻¹) stretch-torsion resonances in the *trans* conformer, but the *gauche* conformer exhibits 22 cm⁻¹ and 14 cm⁻¹ resonances that affect the $\rho_t^{out}(CH_2)$ and the methylene $\rho_w(CH_2)$ fundamentals, respectively. These resonances weakly affect the $\delta_s(CH_3)$ and $\delta^{out}(CH_2)$ fundamentals, which are rather important, and they more strongly affect the highest frequency $\delta(\text{skeletal})$ fundamental, which is the least important of the 9 selected normal coordinates. Through Fermi-coupling, this affects $v_s(CH_2)$ and a'- $v_{as}(CH_3)$, which contribute primarily to the middle region of the spectrum (~2950-3030 cm⁻¹).

A common feature of both conformers is a medium-valued Martin diagnostic (5 cm⁻¹ in *trans* and 8 cm⁻¹ in *gauche*) for the interaction between $v_s(CH_3)$ and $2\tau(CH_3)$. We note that it is commonplace for these kinds of states, *i.e.* a torsional overtone and the corresponding symmetric stretch, to experience strong potential coupling. This is a feature of the rectilinear normal coordinate system.⁶⁵ Because the $v_s(CH_3)$ transition intensity tends to be distributed in the lower

regions of the CH stretch spectrum, we might expect the predictions in that region to be less reliable on account of this.

4. Results and Discussion

- **4.1 Interconversion Potential.** A potential surface for rotation about the central carbon-carbon single bond is given in Figure 1. The potential was generated *via* a Fourier fit to 61 evenly-spaced points at the CCSD(T)/ANO1//CCSD(T)/ANO0 level of theory. Structures of the various stationary points are superimposed. Additionally, each stationary point is labeled with its 0 K enthalpy and 298.15 K free energy, based on the electronic energies from focal point analysis. The interconversion potential and all methyl torsion potentials are shown in the Supporting Information with torsional wavefunctions plotted (Figs. S2, S3, S4, S5, and S6).
- 4.2 Thermochemistry. The results of focal point analyses are found in Tables 1, 2, and 3. These tables report the extrapolated electronic energy differences from *trans*-isoprene (defined as 0) to *gauche*, *gauche* (TS), and *cis* (TS) isoprene, respectively. Calculations of the enthalpy differences are shown below each table. The HF energy differences are seen to converge to within 0.01 kcal/mol on all three tables. The net electron correlation energy converges somewhat slowly (see $+\delta$ [MP2]), but the convergence of correlation energy increments (see $+\delta$ [CCSD] and $+\delta$ [CCSD(T)]) is more rapid. These increments all converge to \pm 0.01 kcal/mol. It is clear that the convergence of the electronic energy is least complete for the *gauche* transition state. Convergence of the MP2 correlation energy is incomplete even with the large cc-pV6Z basis set, and this stationary point also possesses a large (+0.05 kcal/mol) CCSDT(Q) increment. This is not altogether surprising, as transition states often exhibit more multiconfigurational character

than potential minima. It is reasonable then, that more thorough treatments of electron correlation, post-CCSDT(Q), would be necessary to describe it to our desired accuracy.

The cis transition state is comparatively very well-described, showing ± 0.01 kcal/mol convergence by CCSD/cc-pV5Z owing to a cancellation of small, higher-order CC contributions. The superior convergence of the cis TS relative to the gauche TS can be rationalized as due to two competing effects which give rise to these saddle points. 15 Conjugation of the C=C-C=C backbone is stabilizing, and steric repulsion, between hydrogens on separate CH₂ groups, is destabilizing. The *cis* transition state is stabilized by conjugation of its bonds; but by deforming slightly, to gauche with a dihedral angle of 38.7 degrees, it alleviates steric strain and achieves a lower energy. The gauche TS, however, arises from a profound breaking of the π -conjugation. At this geometry, the C=C bonds are nearly orthogonal to each other, τ (C=C-C=C) = 103.6 degrees, the central C-C bond is at its longest, the C=C bonds are shortest, and the electronic structure is quite different. No further discussion of the geometries will be given; however, Cartesian coordinates of the CCSD(T)/ANO1 optimized structures are given in the Supporting Information along with a table of selected internal coordinates (Table S5). The FPA convergence of the gauche minimum is intermediate between the two transition states, and this structure exhibits an intermediate degree of conjugation-breaking. For all stationary points, the contributions from core-correlation (Δ_{core}) and adiabatic corrections (Δ_{DBOC}) are small (≤ 0.01 kcal/mol). Conservative error bars for the relative electronic energies would be ± 0.1 kcal/mol.

Relative enthalpies and free energies of isomerization, in addition to hindered-rotor corrections, are given in Table 5. It can be seen that the 1D variational treatment of the torsional modes leads to large entropic corrections. However, corrections for the methyl torsional degree of freedom are similarly valued for all rotamers; thus, they do not contribute greatly to relative

free energies. This seems reasonable. All four structures possess methyl groups in similar chemical environments. In contrast, the hindered-rotor correction for skeletal torsion increases the entropy of the *gauche* conformer by 0.18 cal/mol·K relative to the *trans* conformer.

Combined with the methyl torsion correction, the net hindered-rotor correction to the entropy is +0.22 cal/mol·K. This stabilizes *gauche*-isoprene by 0.06 kcal/mol relative to *trans*-isoprene, at room temperature. Because the skeletal torsional mode does not contribute to the free-energy of the transition states, the hindered-rotor treatment destabilizes *gauche* (TS) by only 0.02 kcal/mol relative to *trans*. The relative free energy of *cis*-isoprene is insensitive to hindered-rotor treatment.

Our relative 0 K enthalpy and 298.15 K free energies are generally close to the values computed by Allodi and coworkers. ¹³ This is particularly evident for the *trans-cis* differences. In part due to the previously discussed cancellation of higher-order CC contributions and the rapid basis set convergence, our 0 K enthalpy change of 3.35 kcal/mol differs from their result by only about 0.01 kcal/mol, and our 298.15 K free energy change is 3.68 kcal/mol, identical to two decimal places. For the *trans-gauche* interconversion enthalpy, they computed 2.66 kcal/mol, somewhat lower than our 2.82 kcal/mol. Partly due to their harmonic treatment of the torsional contributions, they underestimate the stabilizing effect of free-energy upon *gauche*-isoprene by nearly 0.1 kcal/mol. Overall, our calculations agree that thermal/entropic effects should stabilize *gauche*-isoprene and destabilize both of the transition states, relative to *trans*-isoprene. We stress that the focal point approach allows us to observe the convergence of the electronic energies (the largest contribution to all relative energetics) and to estimate the errors associated with basis set incompleteness and deficiency in electron correlation. The CCSD(T)/aug-cc-pVTZ/BHandHLYP/6-311G** model chemistry used by Allodi and coworkers, chosen for its

suitability not only for isoprene but also for various complexes/adducts with hydroxyl radical, appears to have been a wise choice. However, we feel that our convergent *ab initio* approach, with consideration of anharmonic effects, should be preferred for the isomerization of neat isoprene.

We now consider a comparison of our computed trans-gauche thermochemistry to the experimentally-derived interconversion enthalpy of Squillacote and Liang. 15 In their report, a series of IR spectra were obtained by changing the temperature of the source used to co-deposit isoprene and N₂ onto a cold CsI window. The *trans-gauche* interconversion enthalpy was obtained via a van't Hoff analysis (2.46 kcal/mol), and it was compared to a computed ΔH_0 (2.73 kcal/mol) obtained with the composite G3 method. However, the van't Hoff analysis provides an average interconversion enthalpy, over the range 300-800 K, assuming no isoprene interconversion on the timescale of cooling in the solid-N₂ matrix. To justify direct comparison to their theoretical ΔH_0 value, they noted that (harmonic) thermal corrections to the interconversion enthalpy of (E)-pentadiene were insignificant, never exceeding 0.015 kcal/mol over the same temperature range. We must assume that similar insensitivity was seen for isoprene. This does not agree with our calculations. We predict a far greater temperature dependence in isoprene's ΔH over this range, varying 0.533 kcal/mol in a nonlinear manner (See Figure S7). Furthermore, even harmonic thermal corrections at the CCSD(T)/ANO1 level of theory show a modest temperature dependence, 0.042 kcal/mol, about 3 times higher than what was implied by Squillacote and Liang.¹⁵ We are unconvinced that the experimental number can be meaningfully compared to any 0 K theoretical value. The average (anharmonic) thermal correction over the 300-800 K temperature range is -0.079 kcal/mol. Using this to correct our

0 K value (2.82 kcal/mol), we obtain an average enthalpy change, $\Delta \overline{H}$, of 2.74 kcal/mol. This is 0.28 kcal/mol higher than the experimental value.

Squillacote and Liang reported,¹⁵ for *(E)*-pentadiene, that ΔH varied about \pm 0.3 kcal/mol depending on which *gauche* and *trans* vibrational bands were chosen for van't Hoff analysis. However, they did not report an error bar for their isoprene experiment, and we again assume that a similar deviation was observed. Our $\Delta \overline{H}$ value then falls just within the upper bound of the experimental error bars. As noted above, the error in our calculations is lower than the reported experimental error by at least a factor of three. We suggest that our computed results represent the most accurate thermochemistry on the isoprene system, at present.

4.3 Infrared Spectroscopy. The experimental IR spectrum and VPT2+K simulations for both isoprene rotamers are presented in Figure 2. On the basis of the computed thermodynamics, both *gauche* and *trans* species should contribute to the experimental spectrum; although, *trans* should dominate (97.2% abundance). The spectrum was measured with the quadrupole mass spectrometer tuned to pass ions of only m/z = 67, as described in the Supporting Information. There is generally good agreement between the experimental spectrum and the VPT2+K predictions for the *trans* rotamer; and as discussed below, a few weaker features can be confidently assigned to the *gauche* rotamer. Although the PUC pressure conditions and choice of mass channel minimize the presence of features due to isoprene dimers, some of the weak, broad spectral features are potentially due to these low abundance dimers, which could feasibly have several isomeric structures. The nature of these species is not considered in this report.

The scaled harmonic spectrum of the *trans*-isoprene species (black) is compared to the full VPT2+K treatment (red) in Figure 3. The polyads of a' and a'' symmetry are separated for clarity. It is evident from this comparison that the anharmonic coupling predicted by VPT2+K leads to a spectral complexity in the CH stretch region that disagrees qualitatively with the predictions of the harmonic oscillator model. A detailed discussion of polyad membership is provided in the following section.

4.4 Detailed Spectroscopic Assignments.

4.4.1 Antisymmetric CH₂ Stretches. The two most prominent experimental transitions at 3102 and 3092 cm⁻¹ are clearly assignable to the antisymmetric CH₂ stretches of *trans*-isoprene. The corresponding theoretical transitions fall at 3099 and 3090 cm⁻¹. The higher frequency transition is mostly localized on the vinyl CH₂; whereas, the lower is localized on the methylene CH₂.

There appear to be several more transitions in this region. Comparison to a high temperature scan of this region (Figure 4A) suggests that the small band at 3098 cm⁻¹ and the partially-resolved features at 3096 and 3094 cm⁻¹ derive from the *gauche* conformer. The *gauche* simulation predicts that this region contains multiple resonances, with the vinyl $v_{as}(CH_2)$ being split into peaks at 3095 and 3094 cm⁻¹ via mixing with the nearby [$v_{as}(C=C) + a'' - \delta_{as}(CH_3)$] combination. The methylene $v_{as}(CH_2)$ is 80% pure, having 10% of the [$v_{s}(C=C) + a' - \delta_{as}(CH_3)$] combination. It is predicted at 3091.5 cm⁻¹. An additional feature arises at 3093 cm⁻¹ that borrows small amounts (5%) of both antisymmetric CH_2 stretches, but is primarily [$v_{s}(C=C) + \delta(skeletal) + \rho_{t}(CH_3)$]. This feature loses much of its intensity if Darling-Dennison couplings are

neglected. It seems reasonable that the peak at 3098 cm⁻¹ holds most of the vinyl $v_{as}(CH_2)$ intensity, the shoulder at 3094 cm⁻¹ is the methylene $v_{as}(CH_2)$ fundamental, and the weak feature at 3096 cm⁻¹ is a combination that borrows a bit of intensity from both. Additional features at 3106 and 3090 cm⁻¹ do not have clear assignments. These could correspond to low intensity *trans* features or may be signatures of strong antisymmetric stretches of low-abundance dimers having several conceivable structures.

Most of the remaining transitions are also of mixed character in the simulations, and sometimes the mixing is so extensive that a meaningful description or assignment is not possible. We will move from high to low frequency and focus the discussion on the high intensity features and on those that can be described in less than one paragraph of text.

- **4.4.2 High Frequency Combination Tones.** There are three weak features measured at 3075, 3062, and 3058 cm⁻¹. The *trans* simulation finds three transitions at 3076, 3068, and 3063 cm⁻¹. They all borrow intensity from the out-of-phase vinyl stretch (about 20% in total). Together they participate in a somewhat isolated resonance polyad. Their largest components are 50% [$v_s(C=C) + \delta_s(CH_3)$], 50% [$v_{as}(C=C) + \delta_s(CH_3)$], and 40% [$v_s(C=C) + a'' \rho_r(CH_3) + \rho_w(skeletal)$] respectively. Two transitions are measured at 3050 and 3037 cm⁻¹. Their theoretical counterparts are at 3050 and 3038 cm⁻¹. They are both highly mixed. Intensities come from the in- and out-of-phase vinyl stretches and the symmetric methylene stretch.
- **4.4.3 Middle Region.** The majority (75%) of the intensity of the in-phase vinyl stretch is predicted as a doublet feature at (3025, 3024) cm⁻¹, where it mixes most strongly with the $[\delta_s(CH_3) + v_s(C=C)]$ state. This is in the vicinity of the experimental band at 3021 cm⁻¹. In this

region from about 3010-3030 cm⁻¹, theory predicts roughly the same number of bands as are observed experimentally, but overlap and the variable broadening from the helium makes detailed assignments more difficult. The predicted transition at 3016 cm⁻¹ is roughly 30% of the symmetric methylene stretch and 30% of [$v_{as}(C=C) + \delta^{out}(CH_2)$]. It may correspond to the broad feature at 3018 cm⁻¹.

The region 2970-3000 cm⁻¹ holds four prominent bands around 2981 cm⁻¹. VPT2+K also predicts four bands. The broad doublet feature at (2996, 2993) cm⁻¹ matches most closely to the predictions at (2992, 2987) cm⁻¹. These transitions derive intensity from a mixture of the *a'* - v_{as}(CH₃) and the methylene v_s(CH₂). The intense feature at 2987 cm⁻¹ is predicted at 2982 cm⁻¹ and has the character of 40% *a'*-v_{as}(CH₃) 15% and v^{out}(CH₂). The theory predicts an additional band at 2981 cm⁻¹ comprising 20% *a'*-v_{as}(CH₃) and 25% v^{out}(CH₂). This could either be assigned to the shoulder of the 2987 cm⁻¹ feature or to the smaller, sharper feature at 2981 cm⁻¹, with the nearby intense *gauche* peak assigned to the other. While it is difficult to judge the effect of temperature on intensity where features from multiple conformers overlap, the 2987 and 2981 cm⁻¹ features appear to behave similarly; thus, we assign the shoulder (2985 cm⁻¹) to the *gauche* conformer. This gauche transition is the rather pure (85%) *a'*-like v_{as}(CH₃) fundamental.

4.4.4 Lower Frequency Region. A paradigm shift occurs around 2970 cm⁻¹. For all of the previously discussed transitions, the most significant two- and three-quanta states all involved 1 quantum of C=C stretch excitation and 1-2 quanta of bend excitation. On the lower frequency side of this spectral valley, the important couplings are all to pure bending states. The two CH stretches that contribute to this region are a''- v_{as} (CH₃) and v_{s} (CH₃).

The a'' manifold is far simpler than the a' manifold. We assign the intense transition at 2957 cm⁻¹ to the $v_{as}(CH_3)$ fundamental. In this simulation, it appears at 2958 cm⁻¹ and is 80% pure. It also contains 20% [a'- $\delta_{as}(CH_3) + a''$ - $\delta_{as}(CH_3)$]. An additional band appears at 2896 cm⁻¹ as a result of this Fermi resonance, composed of 10% $v_{as}(CH_3)$ and 60% of the two-quanta scissor combination. This is best assigned to the experimental band at 2890 cm⁻¹. In this region, the *gauche* analog of the a''- $v_{as}(CH_3)$ fundamental has high predicted intensity and thus may be visible in the spectrum. It is predicted at 2950 cm⁻¹ and may be one of the weak features on either side of the *trans* fundamental. Assignment to the 2952 cm⁻¹ feature is most consistent with the theoretical predictions; furthermore, this feature gains intensity at higher isoprene temperatures (Figure 4B).

Lastly $v_s(CH_3)$ is by far the most thoroughly mixed. Its intensity is distributed into various weak transitions between 2970 and 2850 cm⁻¹. None of them can reasonably be called the fundamental transition. The first transition in this polyad is predicted to hold 15% of the intensity and fall at 2950 cm⁻¹. It probably contributes to the broad features underlying the 2940 cm⁻¹ band. The theoretical band at 2938 cm⁻¹ holds 25% of $v_s(CH_3)$ and falls 2 cm⁻¹ to the red of the experimental band center. These two transitions have dark states in common. Their dark-state components are predominantly the a'- $\delta_{as}(CH_3)$ overtone and [a'- $\delta_{as}(CH_3) + \delta(\text{skeletal}) + a'$ - $\rho_t(CH_3)$]. The higher frequency transition is composed of 60% of the three-quanta state, and the lower frequency transition is more mixed: having about 20% of the two-quanta and 30% of the three-quanta components. Figure 4B also reveals a band with a strong temperature dependence at 2932.5 cm⁻¹ Theory predicts a very similar pair of transitions for the *gauche* conformer in this frequency region, composed of zeroth order states that are analogous to those in *trans*. Here, the primarily three-quanta transition falls at 2931 cm⁻¹ with the more mixed transition at 2938 cm⁻¹.

The assignment of this band should be to one of these *gauche* transitions; however, the observation of only a single band here and only one well-defined band for *trans* should cast some doubt upon the validity of the anharmonic coupling picture for this region. Perhaps the mixing between these zeroth-order states is exaggerated here; and in fact, only one transition should possess significant intensity. This experiment cannot confidently answer that question. In this region of the spectrum that contains multiple resonances, discriminating between weak *trans* transitions and strong *gauche* transitions is challenging.

The next notable experimental band is found at 2918 cm⁻¹. The simulation predicts a band at 2913 cm⁻¹ to hold 10% of the $v_s(CH_3)$ intensity. The remaining components of this transition are the overtones of both a'- $\delta_{as}(CH_3)$ and a''- $\delta_{as}(CH_3)$ and three-quanta states connected to them. A doublet is found at (2906, 2905) cm⁻¹. There is a theoretical band at 2902 cm⁻¹, but it is not split. The transition contains 10% $v_s(CH_3)$ and 65% [a''- $\delta_{as}(CH_3)$ + $\rho_w(skeletal)$ + a'- $\rho_r(CH_3)$]. The remaining experimental features are: a broad feature at 2874 and a peak at 2869.5 cm⁻¹ with a shoulder at 2868.5 cm⁻¹. The best match to the broad 2874 cm⁻¹ feature are the overlapping predicted transitions at 2876 cm⁻¹. These are highly mixed, in general and with each other; together they contain 45% [$\delta(CH)$ + $v_{as}(C=C)$], 35% [$v_{as}(C=C)$ + $\rho_w(skeletal)$ + $\rho_w(CH_2)$], and 25% [$\delta^{in}(CH_2)$ + a'- $\delta_{as}(CH_3)$], amongst other things.

The lowest frequency peak and its shoulder match best to the VPT2+K transitions at 2864 and 2862 cm⁻¹ respectively. As with some of the previous transitions, these two share many dark-state components. The primary ones are the overtone of a''- $\delta_{as}(CH_3)$, the combination [a'- $\delta_{as}(CH_3) + \delta^{out}(CH_2)$], and the three-quanta combination [a'- $\delta_{as}(CH_3) + \rho_t^{in}(CH_2) + \rho_t^{out}(CH_2)$]. This feature, with its shoulder, is predicted to hold 20% of the $\nu_s(CH_3)$ intensity.

Overall the predictions in this region are less satisfactory than in other regions of the spectrum. This can be attributed to the inherently higher complexity/dimensionality of the polyads here. There are more states involved, and high accuracy in the force constants becomes more necessary to achieve a qualitatively correct description of the coupling. It is possible that the polyad description needs to be extended even further to include states having 4-quanta of excitation. This is not presently implemented in our VPT2+K scripts. Somewhat more quantifiable than that is the "resonance" between the symmetric stretch and the methyl torsional overtone, as revealed by the Martin diagnostic. This cannot be treated in a satisfying way.

5. Conclusions

In conclusion, a detailed vibrational spectrum has been measured for the CH stretching region of isoprene. The various polyad transitions are well-simulated by the VPT2+K method. Some features in the spectrum are best assigned to the higher energy *gauche* conformer rather than to low intensity combinations/overtones of *trans*. Computations utilizing CBS extrapolation, corrections for post-CCSD(T) correlation, core-correlation, adiabatic effects, and anharmonicity predict respective 0 K and 298.15 K *trans/gauche* energy differences of 2.82 and 2.52 kcal/mol and a room temperature *gauche* population of 2.8%. Hindered-rotor corrections are found to be important for the *trans/gauche* relative free energy, predicting a 0.06 kcal/mol stabilizing effect upon *gauche*-isoprene. These theoretical values are generally in agreement with previous computations, but the error associated with our numbers is lower and more clear. Our *trans* to *gauche* $\Delta \overline{H}$ value over the 300 to 800 K range falls just within the error bar associated with a previously reported experimental interconversion enthalpy. The error in our calculations is lower than the reported experimental error by at least a factor of three. We suggest that our computed

results represent the most accurate thermochemistry on the isoprene system, at present. A rigorous 2D variational treatment of the methyl and skeletal torsional modes would improve upon the separate 1D treatments described in this study. This would eliminate the assumption of uncoupled rotors, allowing for even more confident determinations of the free energy of isomerization.

Supporting Information

Discussion of mass spectrometry and species-selective spectroscopy techniques; discussion of torsional potential energy curves with overlaid eigenstates and wavefunctions; optimized Cartesian coordinates for isoprene stationary points; tables of isoprene thermochemical properties; graph of thermal correction to enthalpy.

Acknowledgements

We acknowledge support from the National Science Foundation (CHE-1664637).

References

- (1) Guenther, A.; Hewitt, C. N.; Erickson, D.; Fall, R.; Geron, C.; Graedel, T.; Harley, P.; Klinger, L.; Lerdau, M.; McKay, W. A., et al., A Global-Model of Natural Volatile Organic-Compound Emissions. *J. Geophys. Res-Atmos.* **1995**, *100*, 8873-8892.
- (2) Chameides, W. L.; Fehsenfeld, F.; Rodgers, M. O.; Cardelino, C.; Martinez, J.; Parrish, D.; Lonneman, W.; Lawson, D. R.; Rasmussen, R. A.; Zimmerman, P., et al., Ozone Precursor Relationships in the Ambient Atmosphere. *J. Geophys. Res-Atmos.* **1992**, *97*, 6037-6055.

- (3) Stone, D.; Evans, M. J.; Edwards, P. M.; Commane, R.; Ingham, T.; Rickard, A. R.; Brookes, D. M.; Hopkins, J.; Leigh, R. J.; Lewis, A. C., et al., Isoprene Oxidation Mechanisms: Measurements and Modelling of OH and HO₂ Over a South-East Asian Tropical Rainforest During the OP3 Field Campaign. *Atmos. Chem. Phys.* **2011**, *11*, 6749-6771.
- (4) Monks, P. S., Gas-Phase Radical Chemistry in the Troposphere. *Chem. Soc. Rev.* **2005**, *34*, 376-395.
- (5) Claeys, M.; Graham, B.; Vas, G.; Wang, W.; Vermeylen, R.; Pashynska, V.; Cafmeyer, J.; Guyon, P.; Andreae, M. O.; Artaxo, P., et al., Formation of Secondary Organic Aerosols Through Photooxidation of Isoprene. *Science* **2004**, *303*, 1173-1176.
- (6) Edney, E. O.; Kleindienst, T. E.; Jaoui, M.; Lewandowski, M.; Offenberg, J. H.; Wang, W.; Claeys, M., Formation of 2-methyl tetrols and 2-methylglyceric acid in Secondary Organic Aerosol from Laboratory Irradiated Isoprene/NO(X)/SO(2)/air Mixtures and their Detection in Ambient PM(2.5) Samples Collected in the Eastern United States. *Atmos. Environ.* 2005, 39, 5281-5289.
- (7) Paulot, F.; Crounse, J. D.; Kjaergaard, H. G.; Kurten, A.; St Clair, J. M.; Seinfeld, J. H.; Wennberg, P. O., Unexpected Epoxide Formation in the Gas-Phase Photooxidation of Isoprene. *Science* **2009**, *325*, 730-733.
- (8) Surratt, J. D.; Murphy, S. M.; Kroll, J. H.; Ng, N. L.; Hildebrandt, L.; Sorooshian, A.; Szmigielski, R.; Vermeylen, R.; Maenhaut, W.; Claeys, M., et al., Chemical Composition of Secondary Organic Aerosol formed from the Photooxidation of Isoprene. *J. Phys. Chem. A* 2006, 110, 9665-9690.
- (9) Kroll, J. H.; Ng, N. L.; Murphy, S. M.; Flagan, R. C.; Seinfeld, J. H., Secondary Organic Aerosol Formation from Isoprene Photooxidation. *Environ. Sci. Technol.* **2006**, *40*, 1869-1877.

- (10) Henze, D. K.; Seinfeld, J. H., Global Secondary Organic Aerosol from Isoprene Oxidation. *Geophys. Res. Lett.* **2006**, *33*, L09812.
- (11) Kleindienst, T. E., Epoxying Isoprene Chemistry. Science 2009, 325, 687-688.
- (12) Greenwald, E. E.; North, S. W.; Georgievskii, Y.; Klippenstein, S. J., A Two Transition State Model for Radical-Molecule Reactions: Applications to Isomeric Branching in the OH-Isoprene Reaction. *J. Phys. Chem. A* **2007**, *111*, 5582-5592.
- (13) Allodi, M. A.; Kirschner, K. N.; Shields, G. C., Thermodynamics of the Hydroxyl Radical Addition to Isoprene. *J. Phys. Chem. A* **2008**, *112*, 7064-7071.
- (14) Compton, D. A. C.; George, W. O.; Maddams, W. F., Conformations of Conjugated Hydrocarbons .1. Spectroscopic and Thermodynamic Study of Buta-1,3-Diene and 2-Methylbuta-1,3-Diene (Isoprene). *J. Chem. Soc. Perk. T* 2 **1976**, 1666-1671.
- (15) Squillacote, M. E.; Liang, F. T., Conformational Thermodynamic and Kinetic Parameters of Methyl-Substituted 1,3-Butadienes. *J. Org. Chem.* **2005**, *70*, 6564-6573.
- (16) Franke, P. R.; Tabor, D. P.; Moradi, C. P.; Douberly, G. E.; Agarwal, J.; Schaefer, H. F.; Sibert, E. L., Infrared Laser Spectroscopy of the n-Propyl and i-Propyl Radicals: Stretch-Bend Fermi Coupling in the Alkyl CH Stretch Region. *J. Chem. Phys.* **2016**, *145*, 224304.
- (17) Schneider, H.; Vogelhuber, K. M.; Schinle, F.; Stanton, J. F.; Weber, J. M., Vibrational Spectroscopy of Nitroalkane Chains Using Electron Autodetachment and Ar Predissociation. *J. Phys. Chem. A* **2008**, *112*, 7498-7506.
- (18) Tabor, D. P.; Hewett, D. M.; Bocklitz, S.; Korn, J. A.; Tomaine, A. J.; Ghosh, A. K.; Zwier, T. S.; Sibert, E. L., Anharmonic Modeling of the Conformation-specific IR Spectra of Ethyl, n-Propyl, and n-Butylbenzene. *J. Chem. Phys.* 2016, 144, 224310.

- (19) Korn, J. A.; Tabor, D. P.; Sibert, E. L.; Zwier, T. S., Conformation-specific Spectroscopy of Alkyl Benzyl Radicals: Effects of a Radical Center on the CH Stretch Infrared Spectrum of an Alkyl Chain. *J. Chem. Phys.* **2016**, *145*, 124314.
- (20) Sibert, E. L.; Kidwell, N. M.; Zwier, T. S., A First-Principles Model of Fermi Resonance in the Alkyl CH Stretch Region: Application to Hydronaphthalenes, Indanes, and Cyclohexane. *J. Phys. Chem. B* **2014**, *118*, 8236-8245.
- (21) Rosnik, A. M.; Polik, W. F., VPT2+K Spectroscopic Constants and Matrix Elements of the Transformed Vibrational Hamiltonian of a Polyatomic Molecule with Resonances Using Van Vleck Perturbation Theory. *Mol. Phys.* **2014**, *112*, 261-300.
- (22) Gonzales, J. M.; Pak, C.; Cox, R. S.; Allen, W. D.; Schaefer, H. F.; Csaszar, A. G.; Tarczay, G., Definitive Ab Initio Studies of Model S(N)2 Reactions CH₃X+F- (X = F, Cl, CN, OH, SH, NH₂, PH₂). *Chem-Eur. J.* **2003**, *9*, 2173-2192.
- (23) Csaszar, A. G.; Allen, W. D.; Schaefer, H. F., In Pursuit of the Ab Initio Limit for Conformational Energy Prototypes. *J. Chem. Phys.* **1998**, *108*, 9751-9764.
- (24) Allinger, N. L.; Fermann, J. T.; Allen, W. D.; Schaefer, H. F., The Torsional Conformations of Butane: Definitive Energetics from Ab Initio Methods. *J. Chem. Phys.* **1997**, *106*, 5143-5150.
- (25) Toennies, J. P.; Vilesov, A. F., Superfluid Helium Droplets: A Uniquely Cold Nanomatrix for Molecules and Molecular Complexes. *Angew. Che. Int. Ed.* **2004**, *43*, 2622-2648.
- (26) Choi, M. Y.; Douberly, G. E.; Falconer, T. M.; Lewis, W. K.; Lindsay, C. M.; Merritt, J. M.; Stiles, P. L.; Miller, R. E., Infrared Spectroscopy of Helium Nanodroplets: Novel Methods for Physics and Chemistry. *Int. Rev. Phys. Chem.* 2006, 25, 15-75.

- (27) Lewerenz, M.; Schilling, B.; Toennies, J. P., A New Scattering Deflection Method for Determining and Selecting the Sizes of Large Liquid Clusters of He-4. *Chem. Phys. Lett.* 1993, 206, 381-387.
- (28) Lewerenz, M.; Schilling, B.; Toennies, J. P., Successive Capture and Coagulation of Atoms and Molecules to Small Clusters in Large Liquid-Helium Clusters. *J. Chem. Phys.* **1995**, *102*, 8191-8207.
- (29) Morrison, A. M.; Liang, T.; Douberly, G. E., Automation of an "Aculight" Continuous-Wave Optical Parametric Oscillator. *Rev. Sci. Instrum.* **2013**, *84*, 013102.
- (30) Chin, S. A.; Krotscheck, E., Systematics of Pure and Doped He-4 Clusters. *Phys. Rev. B* **1995**, *52*, 10405-10428.
- (31) Leavitt, C. M.; Moore, K. B.; Raston, P. L.; Agarwal, J.; Moody, G. H.; Shirley, C. C.; Schaefer, H. F.; Douberly, G. E., Liquid Hot NAGMA Cooled to 0.4 K: Benchmark Thermochemistry of a Gas-Phase Peptide. *J. Phys. Chem. A* **2014**, *118*, 9692-9700.
- (32) Skvortsov, D. S.; Vilesov, A. F., Using He Droplets for Measurements of Interconversion Enthalpy of Conformers in 2-Chloroethanol. *J. Chem. Phys.* **2009**, *130*, 151101.
- (33) Raghavachari, K.; Trucks, G. W.; Pople, J. A.; Headgordon, M., A 5th-Order Perturbation Comparison of Electron Correlation Theories. *Chem. Phys. Lett.* **1989**, *157*, 479-483.
- (34) Hampel, C.; Peterson, K. A.; Werner, H. J., A Comparison of the Efficiency and Accuracy of the Quadratic Configuration-Interaction (QCISD), Coupled Cluster (CCSD), and Brueckner Coupled Cluster (BCCD) Methods. *Chem. Phys. Lett.* **1992**, *190*, 1-12.
- (35) Watts, J. D.; Gauss, J.; Bartlett, R. J., Coupled-Cluster Methods with Noniterative Triple Excitations for Restricted Open-Shell Hartree-Fock and Other General Single Determinant Reference Functions - Energies and Analytical Gradients. *J. Chem. Phys.* 1993, 98, 8718-8733.

- (36) Watts, J. D.; Gauss, J.; Bartlett, R. J., Open-Shell Analytical Energy Gradients for Triple Excitation Many-Body, Coupled-Cluster Methods MBPT(4), CCSD+T(CCSD), CCSD(T), and QCISD(T). *Chem. Phys. Lett.* **1992**, *200*, 1-7.
- (37) Deegan, M. J. O.; Knowles, P. J., Perturbative Corrections to Account for Triple Excitations in Closed and Open-Shell Coupled-Cluster Theories. *Chem. Phys. Lett.* **1994**, 227, 321-326.
- (38) Stanton, J. F., Why CCSD(T) Works: A Different Perspective. *Chem. Phys. Lett.* **1997**, 281, 130-134.
- (39) Almlof, J.; Taylor, P. R., General Contraction of Gaussian-Basis Sets .1. Atomic Natural Orbitals for 1st-Row and 2nd-Row Atoms. *J. Chem. Phys.* **1987**, *86*, 4070-4077.
- (40) CFOUR, A Quantum Chemical Program Package Written by, J. F. Stanton, J. Gauss, M. E. Harding, P. G. Szalay with Contributions from A. A. Auer, R. J. Bartlett, U. Benedikt, C. Berger, D. E. Bernholdt, Y. J. Bomble, et. al., and the Integral Packages Molecule (J. Almlöf and P. R. Taylor), Props (P. R. Taylor), Abacus (T. Helgaker, H. J. Aa. Jensen, P. Jørgensen, and J. Olsen), and ECP Routines by A. V. Mitin and C. Van Wüllen. For the Current Version, see http://www.cfour.de.
- (41) Feller, D., The Use of Systematic Sequences of Wave-Functions for Estimating the Complete Basis Set, Full Configuration-Interaction Limit in Water. *J. Chem. Phys.* **1993**, 98, 7059-7071.
- (42) Helgaker, T.; Klopper, W.; Koch, H.; Noga, J., Basis-Set Convergence of Correlated Calculations on Water. *J. Chem. Phys.* **1997**, *106*, 9639-9646.
- (43) Frisch, J.; Trucks, G. W.; Schlegel, H. B.; Scuseria, G. E.; Robb, M. A.; Cheeseman, J. R.; Scalmani, G.; Barone, V.; Mennucci, B.; Petersson, G. A.; et. al., *Gaussian 09*, Revision E.01; Gaussian, Inc.: Wallingford, CT, USA, 2009.

- (44) Schuurman, M. S.; Allen, W. D.; Schleyer, P. V.; Schaefer, H. F., The Highly Anharmonic BH₅ Potential Energy Surface Characterized in the Ab Initio Limit. *J. Chem. Phys.* **2005**, *122*, 104302.
- (45) Meyer, R.; Gunthard, H. H., General Internal Motion of Molecules Classical Quantum-Mechanical Hamiltonian. *J. Chem. Phys.* **1968**, *49*, 1510-1520.
- (46) Lewis, J. D.; Malloy, T. B.; Chao, T. H.; Laane, J., Periodic Potential Functions for Pseudorotation and Internal-Rotation. *J. Mol. Struct.* **1972**, *12*, 427-449.
- (47) Woon, D. E.; Dunning, T. H., Gaussian-Basis Sets for Use in Correlated Molecular Calculations .5. Core-Valence Basis-Sets for Boron Through Neon. *J. Chem. Phys.* **1995**, *103*, 4572-4585.
- (48) Handy, N. C.; Yamaguchi, Y.; Schaefer, H. F., The Diagonal Correction to the Born-Oppenheimer Approximation Its Effect on the Singlet-Triplet Splitting of CH₂ and Other Molecular Effects. *J. Chem. Phys.* **1986**, *84*, 4481-4484.
- (49) Sellers, H.; Pulay, P., The Adiabatic Correction to Molecular-Potential Surfaces in the SCF Approximation. *Chem. Phys. Lett.* **1984**, *103*, 463-465.
- (50) Boese, A. D.; Oren, M.; Atasoylu, O.; Martin, J. M. L.; Kallay, M.; Gauss, J., W3 Theory: Robust Computational Thermochemistry in the kJ/mol Accuracy Range. *J. Chem. Phys.* **2004**, *120*, 4129-4141.
- (51) Ruden, T. A.; Helgaker, T.; Jorgensen, P.; Olsen, J., Coupled-Cluster Connected-Quadruples Corrections to Atomization Energies. *Chem. Phys. Lett.* **2003**, *371*, 62-67.
- (52) Tajti, A.; Szalay, P. G.; Csaszar, A. G.; Kallay, M.; Gauss, J.; Valeev, E. F.; Flowers, B. A.; Vazquez, J.; Stanton, J. F., HEAT: High Accuracy Extrapolated ab initio Thermochemistry. *J. Chem. Phys.* **2004**, *121*, 11599-11613.

- (53) Kállay, M.; Gauss, J., Approximate Treatment of Higher Excitations in Coupled-Cluster Theory. *J. Chem. Phys.* **2005**, *123*, 214105.
- (54) Kállay, M.; Gauss, J., Approximate Treatment of Higher Excitations in Coupled-Cluster Theory. II. Extension to General Single-Determinant Reference Functions and Improved Approaches for the Canonical Hartree-Fock Case. *J. Chem. Phys.* **2008**, *129*, 144101.
- (55) Bomble, Y. J.; Stanton, J. F.; Kállay, M.; Gauss, J., Coupled-Cluster Methods Including Noniterative Corrections for Quadruple Excitations. *J. Chem. Phys.* **2005**, *123*, 054101.
- (56) MRCC, a quantum chemical program suite written by Kállay, M.; Rolik, Z.; Csontos, J.; Nagy, P.; Samu, G.; Mester, D.; Ladjánszki, I.; Szegedy, L.; Ladóczki, B.; Petrov, K.; et. al. See also. Rolik, Z.; Szegedy, L; Ladjánszki, I.; Ladóczki, B.; Kállay, M. *J. Chem. Phys.* **2013**, *139*, 094105, as well as: www.mrcc.hu.
- (57) McQuarrie, D. A., Statistical Mechanics; Harper Collins: New York, N.Y., 1976, p 641.
- (58) Brown, A. R.; Franke, P. R.; Douberly, G. E., Helium Nanodroplet Isolation of the Cyclobutyl, 1-Methylallyl, and Allylcarbinyl Radicals: Infrared Spectroscopy and Ab Initio Computations. *J. Phys. Chem. A* **2017**, *121*, 7576-7587.
- (59) Nielsen, H. H., The Vibration-Rotation Energies of Molecules. *Rev. Mod. Phys.* **1951**, *23*, 90-136.
- (60) Matthews, D. A.; Vazquez, J.; Stanton, J. F., Calculated Stretching Overtone Levels and Darling-Dennison Resonances in Water: A Triumph of Simple Theoretical Approaches. *Mol. Phys.* 2007, 105, 2659-2666.
- (61) Clabo, D. A.; Allen, W. D.; Remington, R. B.; Yamaguchi, Y.; Schaefer, H. F., A Systematic Study of Molecular Vibrational Anharmonicity and Vibration-Rotation Interaction by Self-Consistent-Field Higher-Derivative Methods - Asymmetric-Top Molecules. *Chem. Phys.* 1988, 123, 187-239.

- (62) Gauss, J.; Stanton, J. F., Analytic CCSD(T) Second Derivatives. *Chem. Phys. Lett.* **1997**, 276, 70-77.
- (63) *Mathematica*, Version 11; Software for Technical Computations; Wolfram Research: Champaign, IL (2016).
- (64) Martin, J. M. L.; Lee, T. J.; Taylor, P. R.; Francois, J. P., The Anharmonic-Force Field of Ethylene, C₂H₄, by Means of Accurate Ab-Initio Calculations. *J. Chem. Phys.* **1995**, *103*, 2589-2602.
- (65) Colbert, D. T.; Sibert, E. L., Variable Curvature Coordinates for Molecular Vibrations. *J. Chem. Phys.* **1989**, *91*, 350-363.

TABLES

TABLE. 1. Incremented FPA of the gauche minimum relative to the trans minimum.

Basis Set	ΔE[HF]	+δ[MP2]	+δ[CCSD]	$+\delta[CCSD(T)]$	+δ[CCSDT]	$+\delta[CCSDT(Q)]$	ΔE[CCSDT(Q)]
ANO0	+2.74	+0.31	-0.39	+0.15	+0.01	+0.02	[+2.84]
cc-pVTZ	+2.74	+0.25	-0.22	+0.15	[+0.01]	[+0.02]	[+2.95]
cc-pVQZ	+2.76	+0.27	-0.23	+0.16	[+0.01]	[+0.02]	[+3.00]
cc-pV5Z	+2.77	+0.30	-0.23	[+0.16]	[+0.01]	[+0.02]	[+3.03]
cc-pV6Z	+2.77	+0.31	[-0.23]	[+0.16]	[+0.01]	[+0.02]	[+3.04]
CBS limit	[+2.77]	[+0.32]	[-0.23]	[+0.16]	[+0.01]	[+0.02]	[+3.06]

 $\Delta H (0K) = \Delta E_{electronic} + \Delta_{ZPVE} + \Delta_{core} + \Delta_{DBOC} = 3.06 - 0.24 + 0.01 + 0.00 =$ **2.82 kcal/mol**

TABLE. 2. Incremented FPA of the gauche TS relative to the trans minimum.

Basis Set	ΔE[HF]	+δ[MP2]	+δ[CCSD]	$+\delta[CCSD(T)]$	+δ[CCSDT]	$+\delta[CCSDT(Q)]$	$\Delta E[CCSDT(Q)]$
ANO0	+5.30	+0.80	-0.82	+0.33	+0.02	+0.05	[+5.69]
cc-pVTZ	+5.40	+0.80	-0.69	+0.34	[+0.02]	[+0.05]	[+5.92]
cc-pVQZ	+5.41	+0.84	-0.68	+0.35	[+0.02]	[+0.05]	[+6.00]
cc-pV5Z	+5.42	+0.86	-0.67	[+0.35]	[+0.02]	[+0.05]	[+6.04]
cc-pV6Z	+5.42	+0.88	[-0.67]	[+0.35]	[+0.02]	[+0.05]	[+6.06]
CBS limit	[+5.43]	[+0.91]	[-0.67]	[+0.35]	[+0.02]	[+0.05]	[+6.09]

 $\Delta H (0K) = \Delta E_{electronic} + \Delta_{ZPVE} + \Delta_{core} + \Delta_{DBOC} = 6.09 - 0.53 + 0.01 + 0.00 =$ **5.57 kcal/mol**

TABLE. 3. Incremented FPA of the cis TS relative to the trans minimum.

Basis Set	ΔE[HF]	+δ[MP2]	+δ[CCSD]	$+\delta[CCSD(T)]$	+δ[CCSDT]	$+\delta[CCSDT(Q)]$	ΔE[CCSDT(Q)]
ANO0	+4.01	-0.10	-0.36	+0.02	-0.02	+0.00	[+3.55]
cc-pVTZ	+4.01	+0.00	-0.33	+0.02	[-0.02]	[+0.00]	[+3.68]
cc-pVQZ	+4.04	+0.02	-0.32	+0.02	[-0.02]	[+0.00]	[+3.74]
cc-pV5Z	+4.04	+0.03	-0.32	[+0.02]	[-0.02]	[+0.00]	[+3.75]
cc-pV6Z	+4.04	+0.03	[-0.32]	[+0.02]	[-0.02]	[+0.00]	[+3.75]
CBS limit	[+4.04]	[+0.03]	[-0.32]	[+0.02]	[-0.02]	[+0.00]	[+3.75]

 $\Delta H (0K) = \Delta E_{electronic} + \Delta_{ZPVE} + \Delta_{core} + \Delta_{DBOC} = 3.75 - 0.41 + 0.01 + 0.01 = 3.35 \text{ kcal/mol}$

TABLE. 4. Qualitative descriptions, symmetries, and CCSD(T)/ANO1 harmonic frequencies and intensities of the normal modes of vibration of *trans*-isoprene.

Mode	Γ	ω (cm ⁻¹)	I (km/mol)	Shorthand	Description	
1	a'	3244.5603	10.6243	$v_{as}(CH_2)$	antisymmetric CH ₂ stretch (vinyl)	
2	a'	3234.3193	9.9565	$v_{as}(CH_2)$	antisymmetric CH ₂ stretch (methylene)	
3	a'	3162.0021	4.1880	ν ⁱⁿ (CH ₂)	symmetric vinyl stretch in-phase	
4	a'	3151.5980	10.2346	v ^{out} (CH ₂)	symmetric vinyl stretch out-of-phase	
5	a'	3144.9542	4.1569	$v_s(CH_2)$	symmetric methylene stretch	
6	a'	3129.8661	15.8022	vas(CH ₃)	antisymmetric CH ₃ stretch	
7	a'	3033.6159	15.8656	v _s (CH ₃)	symmetric CH ₃ stretch	
8	a'	1693.0579	1.4442	$v_s(C=C)$	symmetric C=C stretch	
9	a'	1644.0767	19.5574	$v_{as}(C=C)$	antisymmetric C=C stretch	
10	a'	1503.1165	6.0597	$\delta_{as}(CH_3)$	antisymmetric CH ₃ scissor	
11	a'	1459.0536	1.4189	$\delta^{\rm in}({ m CH_2})$	CH ₂ scissor in-phase	
12	a'	1431.7524	3.1731	$\delta^{\text{out}}(\text{CH}_2)$	CH ₂ scissor out-of-phase	
13	a'	1406.6981	5.6469	$\delta_{\rm s}({ m CH_3})$	CH ₃ symmetric scissor (umbrella)	
14	a'	1334.3384	0.7874	δ(skeletal)	skeletal bend (central)	
15	a'	1314.2937	0.1379	δ(СН)	CH bend	
16	a'	1084.0800	3.1146	$\rho_r(CH_2+CH_3)$	methylene CH ₂ and CH ₃ rock	
17	a'	1004.9739	0.2257	$\rho_r(CH_2+CH_3)$	vinyl CH ₂ and CH ₃ rock	
18	a'	964.4903	0.7134	$v_{as}(C-C)$	antisymmetric C-C stretch	
19	a'	792.1836	0.1036	$v_s(C-C)$	symmetric C-C stretch	
20	a'	527.7516	0.0427	δ(skeletal)	skeletal bend (vinyl, center)	
21	a'	415.9823	1.5062	δ(skeletal)	skeletal bend (methylene, methyl)	
22	a'	277.8314	0.7880	δ(skeletal)	skeletal bend (vinyl, methyl)	
23	a"	3096.7754	13.1548	$v_{as}(CH_3)$	antisymmetric CH ₃ stretch	
24	a"	1484.6844	7.7274	$\delta_{as}(CH_3)$	antisymmetric CH ₃ scissor	
25	a"	1066.1355	0.1490	$\rho_r(CH_3)$	CH ₃ rock	
26	a"	1016.4185	16.9475	δ(CH)	CH bend	
27	a"	923.3859	31.6880	$\rho_{\rm w}({ m CH_2})$	CH ₂ wag (vinyl)	
28	a"	910.7999	40.9321	$\rho_{\rm w}({ m CH_2})$	CH ₂ wag (methylene)	
29	a"	777.5147	0.5691	$\rho_t^{in}(CH_2)$	twisting in-phase (vinyl, methylene)	
30	a"	639.7732	0.2006	$\rho_t^{\text{out}}(\text{CH}_2)$	twisting out-of-phase (vinyl, methylene)	
31	a"	398.5607	9.4163	ρ _w (skeletal)	central carbon wag	
32	a"	213.2430	0.2929	τ(CH ₃)	methyl torsion	
33	a"	157.2597	0.1045	τ(CC)	skeletal torsion	

TABLE. 5. Contributions to the Relative Free Energies (kcal/mol) at 298.15 K.^a

Rotamer	ΔH_0	Evib	δE(CC)	δE(CH ₃)	Svibrot	δS(CC)	δS(CH ₃)	δG	ΔG_{298}
trans	0	1.92	+0.02	+0.07	35.81	+0.11	+0.40	0	0
gauche (TS)	+5.57	1.62	0	+0.07	33.95	0	+0.37	+0.02	+5.84
gauche	+2.82	2.04	+0.03	+0.07	37.04	+0.29	+0.44	-0.06	+2.52
cis (TS)	+3.35	1.57	0	+0.07	33.59	0	+0.44	+0.00	+3.67

^a Enthalpic corrections are given in kcal/mol, and entropic corrections are in cal/mol·K. The δE, δS, and δG quantities are hindered-rotor corrections at 298.15 K, defined as [(hindered-rotor) – (harmonic oscillator)].

FIGURE CAPTIONS

Figure 1. Relaxed torsional potential about the isoprene single C-C bond at the CCSD(T)/ANO1//CCSD(T)/ANO0 level of theory. The energy axis corresponds to the electronic energy differences at this level of theory, but the more rigorous determinations of the 0 K enthalpy and 298.15 K free energy are shown in text for each stationary point (also given in kcal/mol).

Figure 2. Experimental spectrum (black) and theoretical spectra of *trans* (blue) and *gauche* (red) isoprene. The intensities are scaled to reflect the relative populations at room temperature, but *gauche* has been additionally magnified three times to improve visibility.

Figure 3. Comparison of scaled CCSD(T)/ANO1 harmonic frequencies with VPT2+K frequencies, separated by symmetry, for *trans*-isoprene. The scaling factor is chosen to best match the experimental antisymmetric CH₂ stretch frequencies.

Figure. 4. (a) Comparison of antisymmetric stretching region with isoprene samples at approximately 300 K (black) and 700 K (red). The spectra are scaled to maximize the overlap of the intense *trans* transitions at 3092 and 3102 cm⁻¹. (b) Comparison of lower frequency region with isoprene samples at approximately 300 K (black) and 700 K (red). The spectra are scaled to maximize the overlap of the *trans* fundamental at 2958 cm⁻¹. Candidate *gauche* bands are indicated by the black arrows.

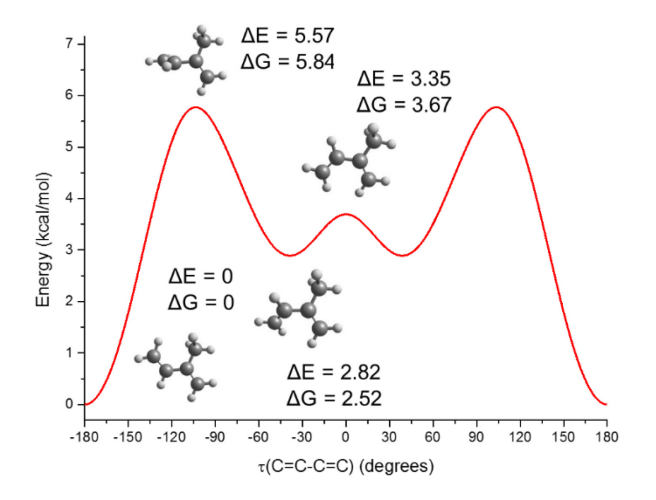


Figure 1

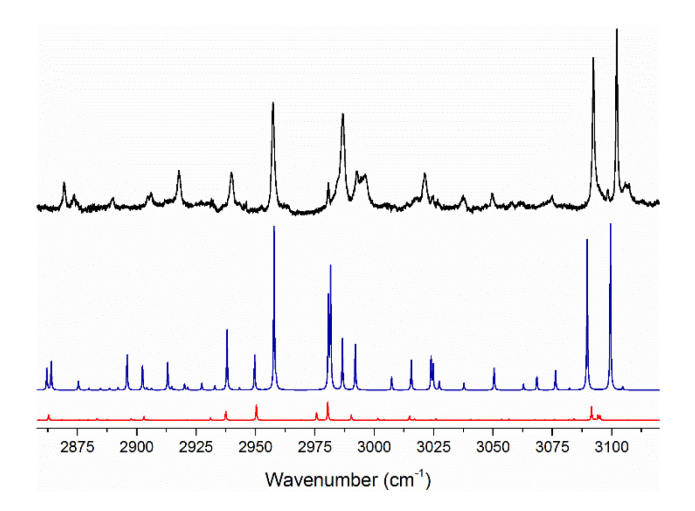


Figure 2

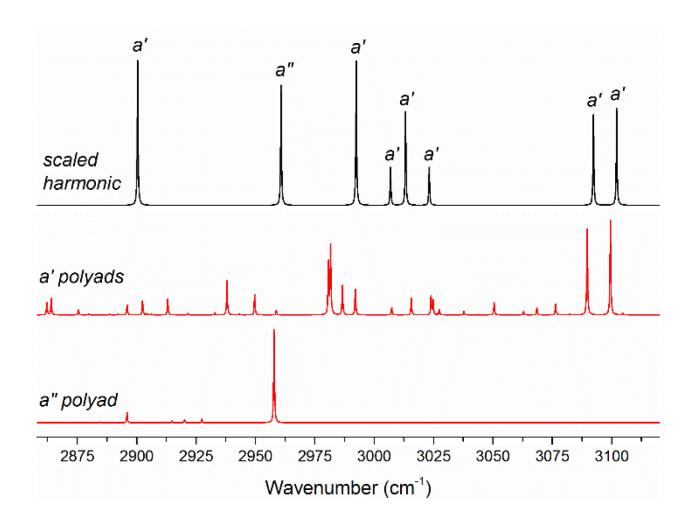


Figure 3

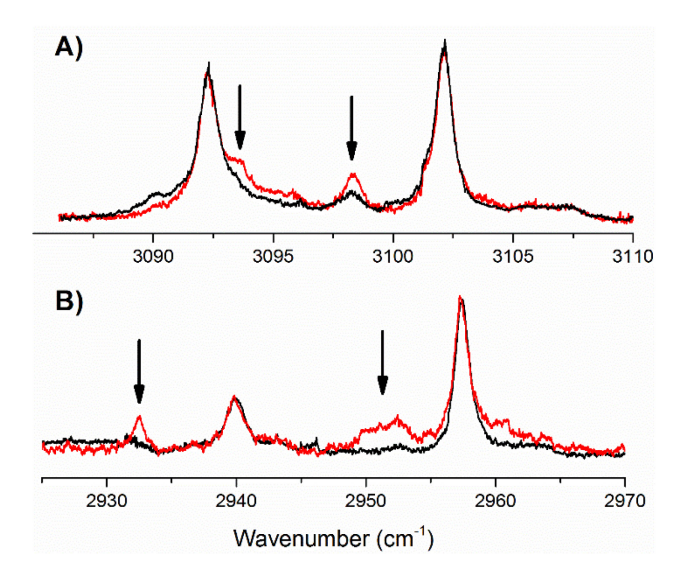


Figure 4

TOC GRAPHIC

